Molecular Therapy
Nucleic Acids
Original Article

Notochordal-Cell-Derived Exosomes Induced by Compressive Load Inhibit Angiogenesis via the miR-140-5p/Wnt/β-Catenin Axis

Zhen Sun,[1,6] Bing Liu,[2,6] Zhi-Heng Liu,[3] Wen Song,[4] Dong Wang,[1] Bei-Yu Chen,[1] Jing Fan,[1] Zhe Xu,[5] Dan Geng,[1] and Zhuo-Jing Luo[1]

[1]Department of Orthopedic, Xijing Hospital, Fourth Military Medical University, Western Changle Road, Xi'an 710032, China; [2]Department of Radiology, Xijing Hospital, Fourth Military Medical University, Western Changle Road, Xi'an 710032, China; [3]Department of Orthopedic, 986 Air Force Hospital of China, Xi'an 710032, China; [4]State Key Laboratory of Military Stomatology & National Clinical Research Center for Oral Diseases & Shaanxi Key Laboratory of Oral Diseases, Department of Prosthodontics, School of Stomatology, The Fourth Military Medical University, Xi'an 710032, China; [5]Student Brigade, Fourth Military Medical University, Western Changle Road, Xi'an 710032, China

Angiogenesis is a pathological signature of intervertebral disc degeneration (IDD). Accumulating evidence has shown that notochordal cells (NCs) play an essential role in maintaining intervertebral disc development and homeostasis with inhibitive effect on blood vessel in-growth. However, the anti-angiogenesis mechanism of NCs is still unclear. In the current study, we, for the first time, isolated NC-derived exosomes (NC-exos) and showed their increased concentration following compressive load cultures. We further found that NC-exos from 0.5 MPa compressive load cultures (0.5 MPa/NC-exos) inhibit angiogenesis via transferring high expressed microRNA (miR)-140-5p to endothelial cells and regulating the downstream Wnt/β-catenin pathway. Clinical evidence showed that exosomal miR-140-5p expression of the nucleus pulposus is negatively correlated with angiogenesis in IDD. Finally, 0.5 MPa/NC-exos were demonstrated to have a therapeutical impact on the degenerated disc with an anti-angiogenesis effect in an IDD model. Consequently, our present findings provide insights into the anti-angiogenesis mechanism of NC-exos, indicating their therapeutic potential for IDD.

INTRODUCTION

Intervertebral disc (IVD) degeneration (IDD) and related diseases are important contributors to low back pain, which affects almost 80% of the population at least one time during their life. Studies have shown that the cause of IDD is multifactorial with various leading factors. Previously, we elucidated the immune privilege of the intervertebral disc with respect to various pathways.[1–4] As the largest avascular organ of the body, the intervertebral disc consists of the inner nucleus pulposus (NP), the surrounding annulus fibrosus (AF), and the adjacent cartilaginous endplates. The healthy disc is characterized with limited blood vessels in the outer surface of the AF. In IDD, vascular invasion was widely observed and was thought to play an important role in IDD progress by bringing activated immunocytes and inflammatory cytokines, facilitating neuralization, and thus breaking the homeostasis of the disc. However, the mechanism of how healthy intervertebral disc inhibits vascularization is still unclear.

During the embryogenesis period, the rod-like notochord is entrapped from the vertebral body and develops to the NP tissue soon in the early fetal life, whereas blood vessels recede from the inner area. The large, vacuolated notochordal cells (NCs) thus remain in the NP tissue. During the second decade of human life, the population of NCs starts to decrease, and early IDD happens. Accumulating evidence has demonstrated that NCs play an essential role in disc development and function.[5,6] Particularly, NCs were shown not only to activate NP cells (NPs)[7] and mesenchymal stem cells (MSCs)[8] but also to inhibit blood vessel in-growth.[9] Therefore, NCs have received considerable attention due to their therapeutic potential. However, the anti-angiogenesis effects of NCs in the disc are still unclarified.

Exosomes are extracellular vesicles with a range of 30–150 nm in diameter, secreted by many cell types, including stem cells, tumor cells, immunocytes, and chondrocytes.[10] The transfer of numerous bioactive substances, such as cytokines, proteins, lipids, and RNAs, is generally defined as intercellular communicating vehicles. It has been shown that exosomes play an essential role in tumor metastasis,[11] immunomodulation,[12] osteoarthritis,[13] and angiogenesis.[14] However, no studies showed whether NCs produce exosomes and their impact on disc homeostasis.

Received 4 August 2020; accepted 13 October 2020;
https://doi.org/10.1016/j.omtn.2020.10.021.

[6]These authors contributed equally to this work.

Correspondence: Zhen Sun, Department of Orthopedic, Xijing Hospital, Fourth Military Medical University, Western Changle Road, Xi'an 710032, China.
E-mail: fmmusz@126.com
Correspondence: Zhuo-Jing Luo, Department of Orthopedic, Xijing Hospital, Fourth Military Medical University, Western Changle Road, Xi'an 710032, China.
E-mail: zjluo@fmmu.edu.cn

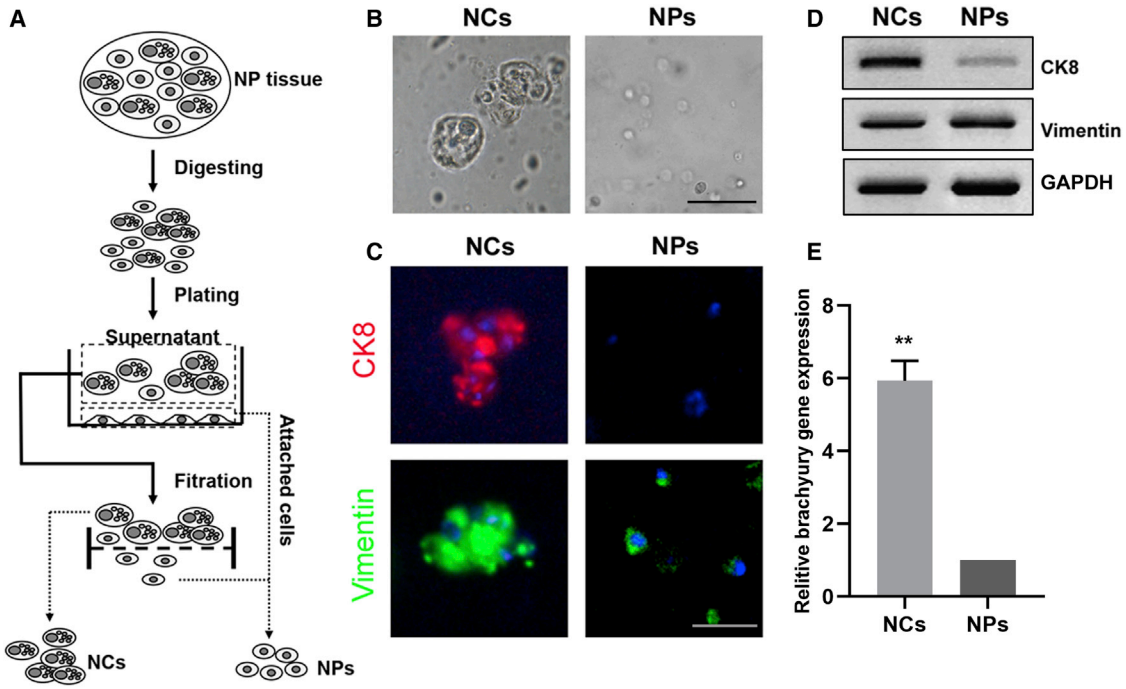

Figure 1. Identification of Notochordal Cells (NCs)

(A) Schematic diagram for isolation of NCs and chondrocyte-like nucleus pulposus cells (NPs). (B) Isolated NCs and NPs. Bar, 50 μm. (C) Immunofluorescence staining of cytokeratin 8 (CK8) and vimentin expression in NCs and NPs. Bar, 50 μm. (D) Western blotting analysis of CK8 and vimentin expression in NCs and NPs. (E) RT-PCR analysis of brachyury expression in NCs and NPs. The expression of brachyury in NPs was normalized to 1. Mean ± SEM is provided (n = 3). **$p < 0.01$.

In the current study, we hypothesized that NCs could secret NC-derived exosomes (NC-exos) and the NC-exos might be impacted by compressive load considering the close relation of NCs and biomechanics. In addition, the NC-exos might play an important role in disc angiogenesis inhibition via delivering a bioactive substance to vascular endothelial cells. The elucidation of these effects might shed light on the mechanism of NCs' application in IDD treatment.

RESULTS

Identification of NCs

NCs and NPs were isolated and obtained with the mentioned filtration procedure. As shown in Figure 1B, isolated NCs were presented as large cells with heterogeneous vacuole-like structures, and NPs are smaller spherical cells. We then examined the cells with the notochordal marker cytokeratin 8 (CK8) and mesenchymal marker vimentin. As shown in Figure 2C, NCs were observed as dense clusters, which were both CK8 and vimentin positive, whereas NPs were only vimentin positive. Western blotting demonstrated the same tendency expression of these markers in NCs and NPs (Figure 1D). Additionally, RT-PCR showed that NCs brachyury gene expression was significantly higher than that of NPs (Figure 1E).

NC-Exos Isolation and Their Response to Compressive Loads

To explore the existence and potential functions of NC-exos, exosome extraction procedures were performed with NC conditioned media (Figure 2A). NC-exos were identified as membrane-encapsulated particles by transmission electron microscopy (TEM) (Figures 2B and 2C), and their size and shape were approximately a size of 50–150 nm in diameter (Figure 2D). A 3hree-dimensional plot of relative intensity showed a stereo picture of the size distribution (Figure 2E). NC-exos expressed exosomal positive marker proteins CD63 and Tsg101. Additionally, calnexin expressed in endoplasmic reticulum is negatively expressed in NC-exos (Figure 2F). To evaluate the impact of NC-exos on angiogenesis, NC-exos were further used in endothelial cell cultures. NC-exos were labeled with PKH67 and incubated in human umbilical vein endothelial cells (HUVECs) culture. Fluorescent microscopy and flow cytometry results demonstrated that PKH26-labeled NC-exos were internalized by HUVECs (Figures 2G and 2H). It has been shown that NCs responded to mechanical stress with various effects, such as vacuolation exhaustion and proteoglycan-matrix secretion.[15] Here, we detected the impact of compressive loads on NC-exos. NCs were cultured in different compressive loads, and NC-exos were extracted and analyzed. NCs exhibited increased NC-exos concentration after compressive load cultures (Figure 2J). However, no significant difference was observed in cell viability after compressive load cultures (Figure 2K).

0.5. MPa/NC-Exos Inhibit Angiogenesis

To evaluate the impact of NC-exos on angiogenesis, NC-exos derived from different compressive load cultures were used for angiogenesis

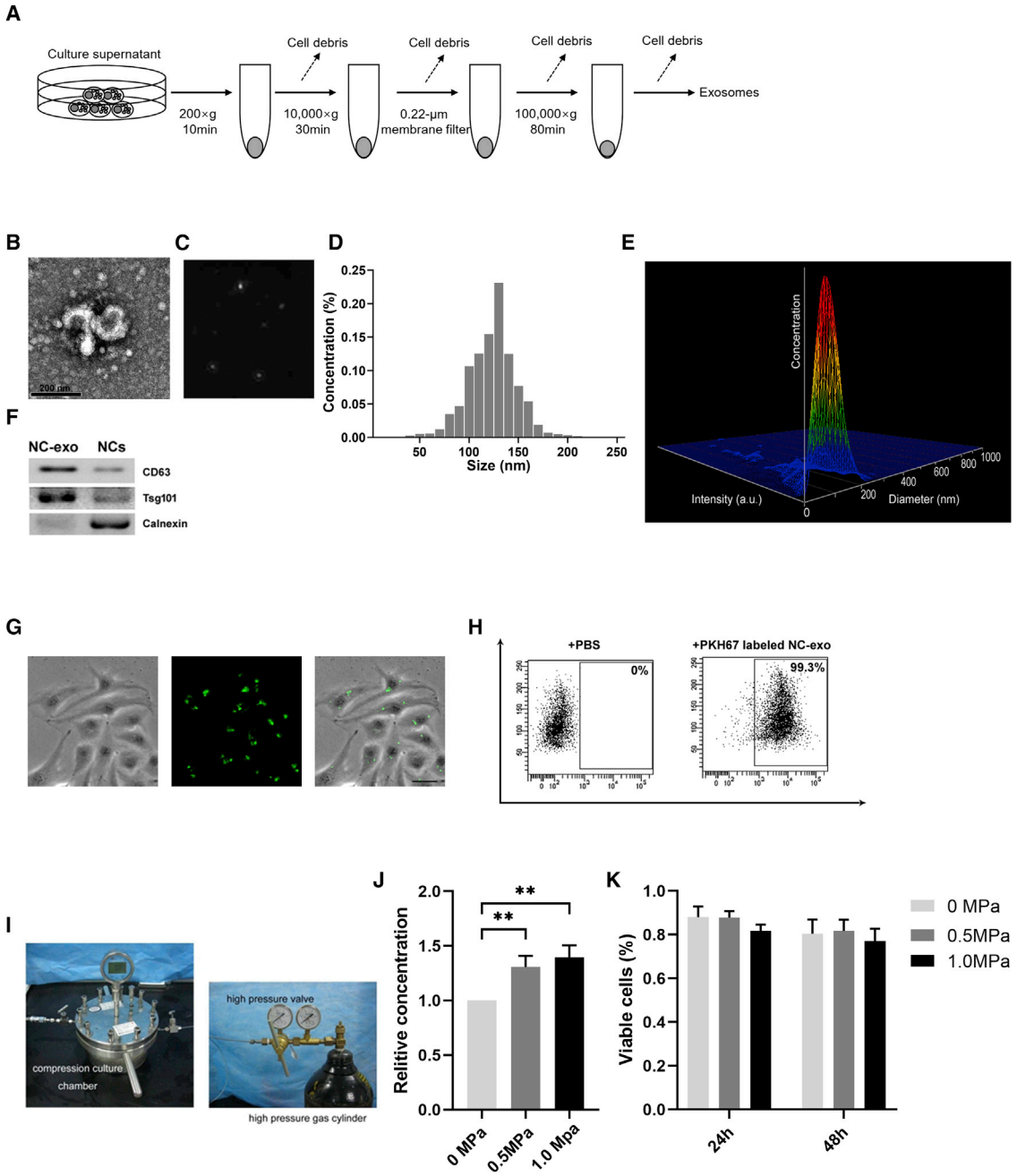

Figure 2. NC-Derived Exosomes (NC-Exos) Isolation and Their Response to Compressive Loads

(A) Schematic diagram for isolation of NC-exos. (B) Typical image of NC-exos morphology was captured by transmission electron microscopy (TEM). (C) Nanoparticle tracking measurements under flow conditions with the corresponding video frame. (D) Particle size distribution of NC-exos was examined by nanoparticle trafficking analysis. (E) Three-dimensional plot of relative intensity showed the size distribution of NC-exos in the stereo picture. (F) Western blotting analysis of exosomal-positive markers (CD63 and Tsg101) and negative protein calnexin from NC-exos. (G) Observation of human umbilical vein endothelial cells (HUVECs) incubated with PKH67-labeled NC-exos. The green fluorescence in HUVECs indicated cellular internalization of NC-exos. Bar, 10 μm. (H) Flow cytometry assay showed the percentage of green fluorescence-positive HUVECs after incubation with PBS or PKH67-labeled NC-exos. (I) Schematic diagram for the compressive load culture system. (J) Relative concentration of NC-exos from compressive load-cultured NCs. The concentration of NC-exos without compressive load culture was normalized to 1. Mean ± SEM is provided (n = 3). **$p < 0.01$. (K) Viability of NCs following 0 MPa, 0.5 MPa, and 1.0 MPa cultures at 24 h and 48 h. No significant difference of cell viability was observed in applied compressive loads.

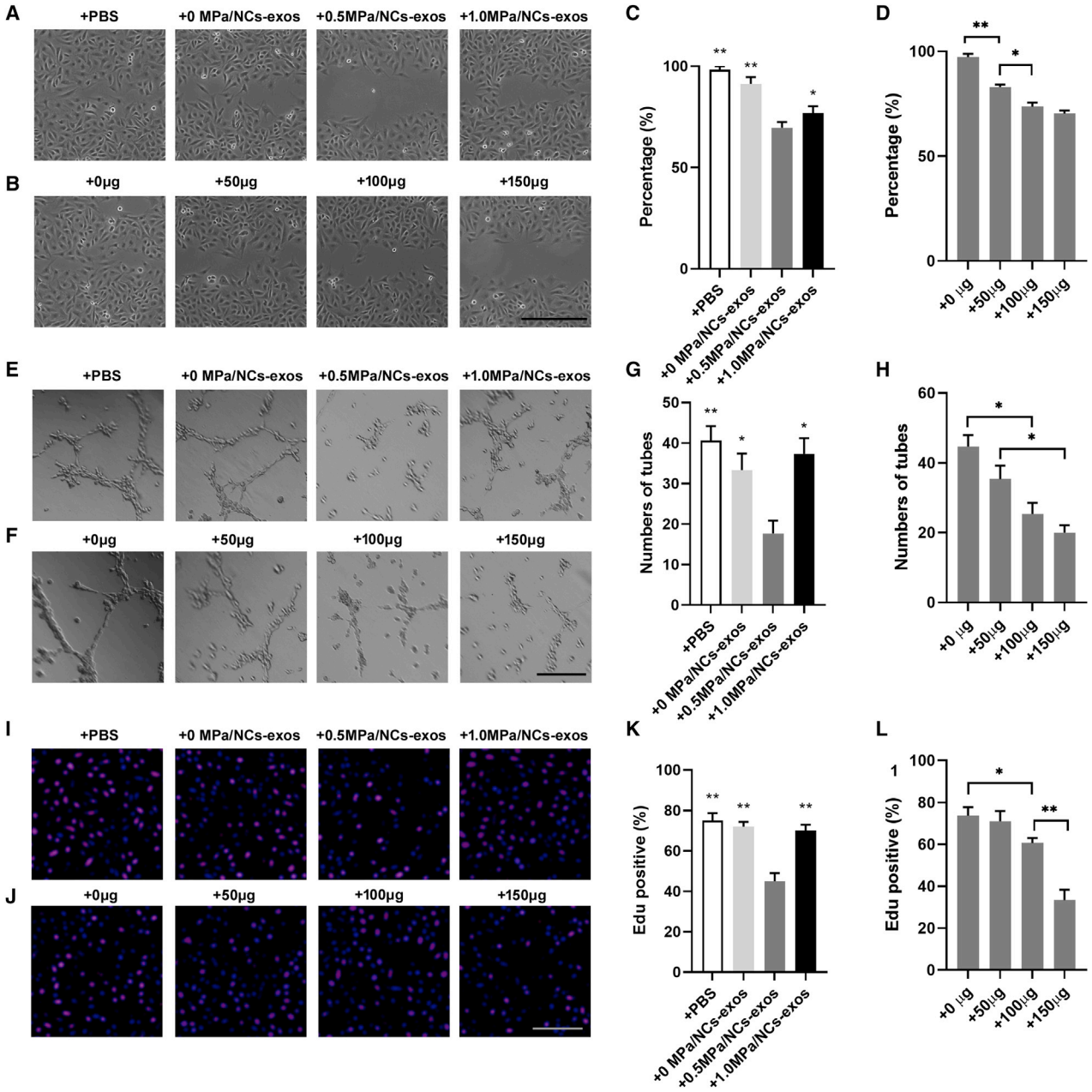

Figure 3. 0.5 MPa/NC-Exos Inhibit Angiogenesis

(A and C) Effect of 0 MPa/NC-exos, 0.5 MPa/NC-exos, and 1.0 MPa/NC-exos on migration of HUVECs. Bar, 100 μm. Mean ± SEM is provided (n = 3). *p < 0.05, **p < 0.01 for comparison with the 0.5-MPa/NC-exos group. (B and D) Effect of 0 μg, 50 μg, and 100 μg 0.5 MPa/NC-exos on migration of HUVECs. Bar, 100 μm. Mean ± SEM is provided (n = 3). *p < 0.05, **p < 0.01. (E and G) Effect of 0 MPa/NC-exos, 0.5 MPa/NC-exos, and 1.0 MPa/NC-exos on the tube formation ability of HUVECs. Bar, 100 μm. Mean ± SEM is provided (n = 3). *p < 0.05, **p < 0.01 for comparison with the 0.5-MPa/NC-exos group. (F and H) Effect of 0 μg, 50 μg, and 100 μg 0.5 MPa/NC-exos on the tube formation ability of HUVECs. Bar, 100 μm. Mean ± SEM is provided (n = 3). *p < 0.05, **p < 0.01. (I and K) Effect of 0 MPa/NC-exos, 0.5 MPa/NC-exos, and 1.0 MPa/NC-exos on proliferation of HUVECs. Bar, 100 μm. Mean ± SEM is provided (n = 3). *p < 0.05, **p < 0.01 for comparison with the 0.5-MPa/NC-exos group. (J and L) Effect of 0 μg, 50 μg, and 100 μg 0.5 MPa/NC-exos on proliferation of HUVECs. Bar, 100 μm. Mean ± SEM is provided (n = 3). *p < 0.05, **p < 0.01.

examination in the endothelial cell. As was shown in Figures 3A and 3C, treatment with 0.5 MPa/NC-exos dramatically inhibited migration of HUVECs compared with other groups. Moreover, 0.5 MPa/NC-exos showed a dose-dependent inhibitive effect on migration of HUVECs (Figures 3B and 3D). Moreover, 0.5 MPa/NC-exos showed an inhibitive angiogenesis effect in the tube formation assay (Figures

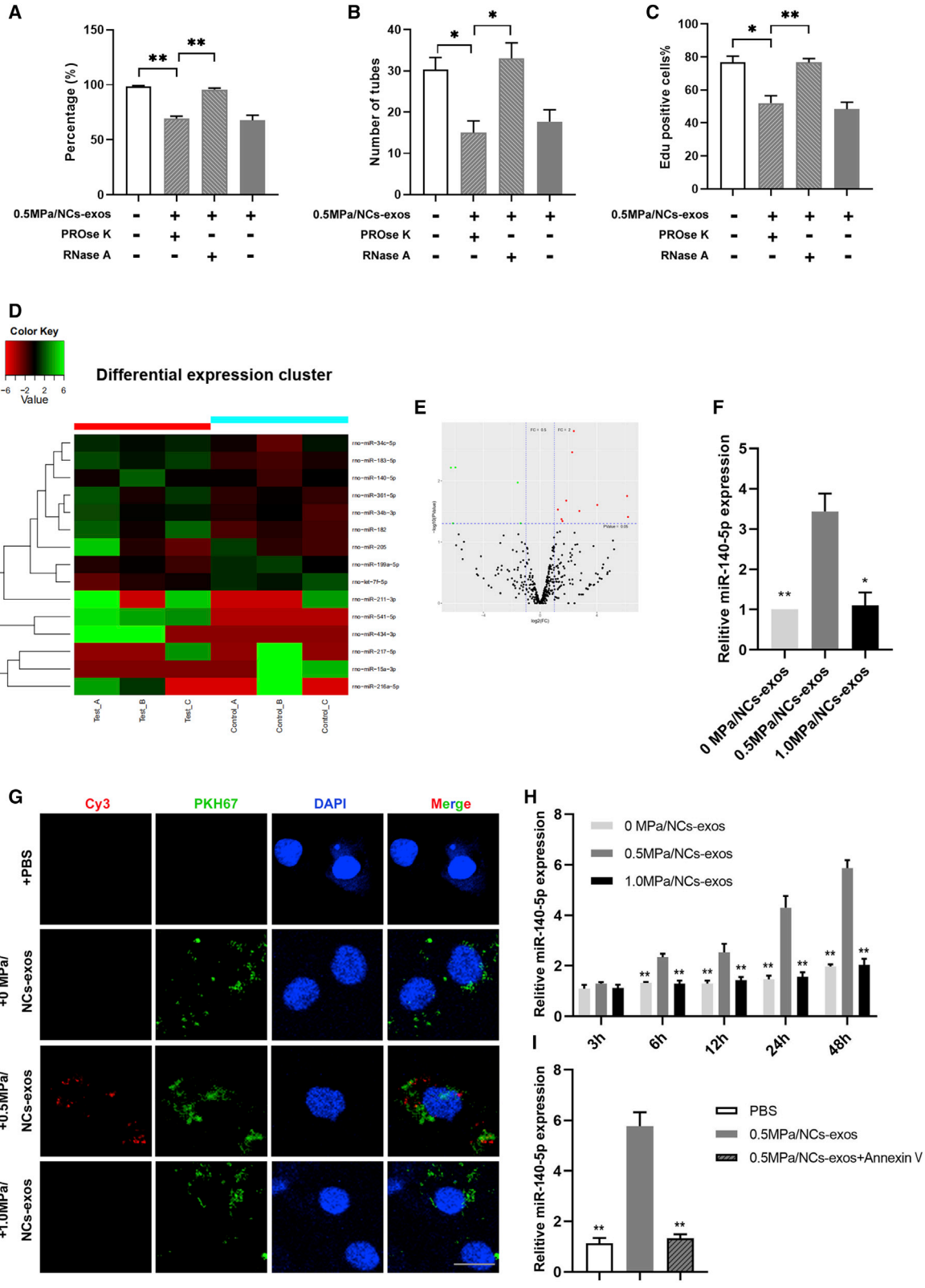

(legend on next page)

3E–3H). In addition, cell proliferation was suppressed by 0.5 MPa/NC-exos (Figures 3I–3L). These data suggest that NC-exos induced by a 0.5-MPa compressive load inhibit endothelial cell angiogenesis.

MicroRNA (miR)-140-5p Is Transferred by 0.5 MPa/NC-Exos to Endothelial Cells and Inhibits Angiogenesis

To explore the effective components of the 0.5-MPa/NC-exos in anti-angiogenesis effects, pretreatment of PROse K (proteinase K) or RNase A was used to exclude the influence of proteins or RNAs. As shown in Figures 4A–4C, RNase A pretreated 0.5 MPa/NC-exos showed an attenuated, inhibitive effect on endothelial cell migration, angiogenesis, and proliferation, whereas PROse K pretreatment showed no significant effect compared to the untreated group, suggesting that RNAs play an important role in the anti-angiogenic effect of 0.5 MPa/NC-exos. Studies have shown that exosomes are effective carriers, transferring microRNAs (miRNAs) from cells to cells. Thus, we hypothesized that miRNAs be transferred from NCs to endothelial cells via NC-exos. To identify potential anti-angiogenic-associated miRNAs in 0.5 MPa/NC-exos, an miRNA array was performed using NC-exos with or without 0.5 MPa culture. Among the differently expressed miRNAs, ten miRNAs (miR-140-5p, miR-182, miR-183-5p, miR-205, miR-211-3p, miR-34b-3p, miR-34c-5p, miR-361-5p, miR-434-3p, and miR-541-5p) were significantly upregulated. The heatmap indicates the result of a two-way hierarchical clustering of miRNAs (Figure 4D). Volcano plots showed 10 upregulated and 5 downregulated miRNAs (Figure 4E). To evaluate the effect of upregulated miRNAs on angiogenesis, the miRNAs were overexpressed in HUVECs, respectively. Among these miRNAs, the upregulation of miR-140-5p showed a significant inhibitive effect on angiogenesis in endothelial cells (Figure S1). The expression of miR-140-5p in 0.5 MPa/NC-exos was confirmed (Figure 4F). Then, NCs were transfected with Cy3-labeled miR-140-5p mimics and cultured in compressive loads, and the NC-exos were labeled by PKH67 and incubated with HUVECs. As demonstrated in Figure 4G, HUVECs showed both Cy3 and PKH67 fluorescence positive in the 0.5-MPa/NC-exos group, whereas HUVECs showed only PKH67 fluorescence in 0 MPa and 1.0 MPa groups. Then, the miR-140-5p expression in HUVECs was examined, and RT-PCR results showed that HUVECs demonstrated an increased level of miR-140-5p after incubation with 0.5 MPa/NC-exos, whereas no miR-140-5p upregulation was detected in other groups (Figure 4H). With the application of Annexin V, an exosome internalization inhibitor, 0.5 MPa/NC-exos lost the ability to upregulate miR-140-5p expression in HUVECs (Figure 4I). Collectively, these results indicate that miR-140-5p is the main contributor in the anti-angiogenesis effect in 0.5 MPa/NC-exos.

miR-140-5p Regulates Anti-angiogenesis via Its Functional Target Wnt11

To evaluate how miR-140-5p regulates the anti-angiogenesis mechanism, three mRNA target-predicting algorithms (miRDB, miRWalk, and TargetScan) were used to recognize the potential downstream targets of miR-140-5p. Among the potential targets, Wnt11 was overlapped in all databases (Figure 5A). To detect whether Wnt11 is a target of miR-140-5p, 3′ UTRs of Wnt11 were cloned into the luciferase plasmid psiCHEK-2 in HEK293A and HUVECs. Notably, the luciferase activities of 3′ UTR of Wnt11 were suppressed by miR-140-5p (Figure 5B). We then examined the expression of Wnt/β-catenin in HUVECs nuclear and cytoplasm. As shown in Figure 5C, overexpression of miR-140-5p in HUVECs downregulated Wnt11 expression and inhibited β-catenin nuclear accumulation, whereas restoration of Wnt11 expression abrogated these effects. Additionally, we also examined the levels of matrix metalloproteinases (MMPs) in HUVEC cultures due to their close relationship with Wnt/β-catenin regulation. As expected, the levels of MMP-2 and MMP-7 were downregulated in miR-140-5p-overexpressed HUVEC cultures, whereas restoration of Wnt11 restored their expression (Figure 5D). Furthermore, overexpression of miR-140-5p inhibited HUVEC migration, tuber formation, and proliferation, and restoration of Wnt11 abolished miR-140-5p-induced angiogenesis inhibition (Figures 5E–5J).

0.5. MPa/NC-Exos Silence Wnt11 and Inhibit Angiogenesis in HUVECs

To explore the impact of 0.5 MPa/NC-exos on endothelial cells, we detected whether 0.5 MPa/NC-exos silence Wnt11 and thus inhibit angiogenesis of HUVECs. The luciferase activity of Wnt11 3′ UTR was reduced by 0.5 MPa/NC-exos but not 0 MPa/NC-exos or 1.0 MPa/NC-exos. Moreover, the addition of the miR-140-5p inhibitor or exosome internalization inhibitor, Annexin V, showed restored luciferase activity of Wnt11 3′ UTR, suggesting that Wnt11 in HUVECs can be silenced by miR-140-5p derived from 0.5 MPa/NC-exos (Figure 6A). Then, Wnt/β-catenin expression was examined in 0.5 MPa/NC-exo-cultured HUVECs. As shown in Figure 7B, 0.5

Figure 4. miR-140-5p Is Transferred by 0.5 MPa/NC-Exos to Endothelial Cells and Inhibits Angiogenesis

(A) Effect of 0.5 MPa/NC-exos, 0.5 MPa/NC-exos + PROse K, and 0.5 MPa/NC-exos + RNase A on migration of HUVECs. Mean ± SEM is provided (n = 3). **p < 0.01. (B) Effect of 0.5 MPa/NC-exos, 0.5 MPa/NC-exos + PROse K, and 0.5 MPa/NC-exos + RNase A on tube formation ability of HUVECs. Mean ± SEM is provided (n = 3). *p < 0.05. (C) Effect of 0.5 MPa/NC-exos, 0.5 MPa/NC-exos + PROse K, and 0.5 MPa/NC-exos + RNase A on proliferation of HUVECs. Mean ± SEM is provided (n = 3). *p < 0.05, **p < 0.01. (D) Heatmap diagram of differential miRNA expression between 0 MPa/NC-exos and 0.5 MPa/NC-exos. Red, increased expression; green, decreased expression. (E) Volcano plots of differentially expressed miRNAs. Red, increased expression; green, decreased expression; and black, no difference. p < 0.05 and fold change > 2 was considered significant. (F) RT-PCR validated the increased expression of miR-140-5p in 0.5 MPa/NC-exos. Mean ± SEM is provided (n = 3). *p < 0.05, **p < 0.01 for comparison with the 0.5-MPa/NC-exos group. (G) Observation of Cy3 fluorescence and PKH67 lipid dye in HUVECs after adding PKH67-labeled NC-exos for 48 h. Bar, 10 μm. (H) RT-PCR analysis of miR-140-5p expression in HUVECs incubated with 0 MPa/NC-exos, 0.5 MPa/NC-exos, and 1.0 MPa/NC-exos for 3 h, 6 h, 12 h, 24 h, and 48 h. Mean ± SEM is provided (n = 3). *p < 0.05, **p < 0.01 for comparison with the 0.5-MPa/NC-exos group. (I) RT-PCR analysis of miR-140-5p expression in HUVECs incubated with 0.5 MPa/NC-exos or 0.5 MPa/NC-exos + Annexin V for 48 h. Mean ± SEM is provided (n = 3). *p < 0.05, **p < 0.01 for comparison with the 0.5-MPa/NC-exos group. n = 3 means cells isolated of 3 individuals.

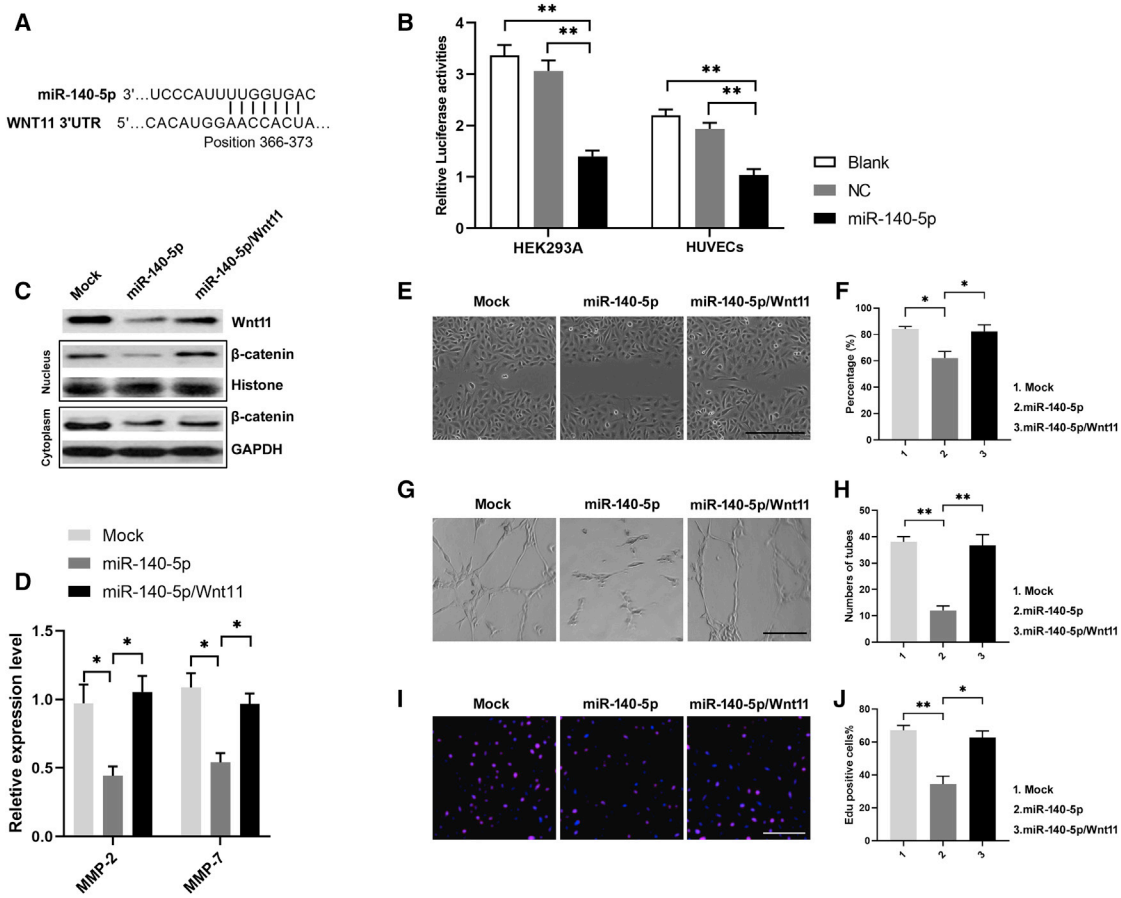

Figure 5. miR-140-5p Regulates Anti-Angiogenesis via Its Functional Target Wnt11

(A) Potential miR-140-5p binding site in the WNT11 3′ UTR predicted by TargetScan. (B) Luciferase activities of 3′ UTR WNT11-luciferase (luc) constructs in HEK293A and HUVECs after transfection of miR-25-3p mimics. Mean ± SEM is provided (n = 3). *p < 0.05, **p < 0.01. (C) Western blotting assay showed Wnt11 expression and β-catenin expression in nucleus/cytoplasm in miR-140-5p overexpressing or miR-140-5p/Wnt11 coexpressing HUVECs. (D) ELISA detection showed the levels of matrix metalloproteinase (MMP)-2 and MMP-7 in medium of miR-140-5p overexpressing or miR-140-5p/Wnt11 coexpressing HUVECs. Mean ± SEM is provided (n = 3). *p < 0.05, **p < 0.01. (E and F) Effects of miR-140-5p and miR-140-5p/Wnt11 on migration of HUVEC monolayers. Bar, 100 μm. Mean ± SEM is provided (n = 3). *p < 0.05, **p < 0.01. (G and H) Effects of miR-140-5p and miR-140-5p/Wnt11 on tube formation ability of HUVECs. Bar, 100 μm. Mean ± SEM is provided (n = 3). *p < 0.05, **p < 0.01. (I and J) Effects of miR-140-5p and miR-140-5p/Wnt11 on proliferation of HUVECs. Bar, 100 μm. Mean ± SEM is provided (n = 3). *p < 0.05, **p < 0.01.

MPa/NC-exos dramatically decreased the expression of Wnt11 and inhibited β-catenin nuclear accumulation. The application of Annexin V or miR-140-5p inhibitor abrogated these effects. Similarly, restored Wnt11 expression rescued β-catenin nuclear accumulation (Figures 6B and 6C). In addition, the levels of MMP-2 and MMP-7 were downregulated in 0.5 MPa/NC-exo-treated HUVEC cultures, whereas the addition of Annexin V, miR-140-5p inhibitor, or restored Wnt11 increased their levels (Figure 6D). *In vitro* migration assay, tube formation assay, and proliferation assay showed that the treatment of 0.5 MPa/NC-exos inhibited angiogenesis, whereas miR-25-3p inhibitor or Annexin V alleviated their function in promoting angiogenesis. Additionally, Wnt11 restoration in recipient cells suppressed these effects (Figures 6E–6H). These results suggest that 0.5 MPa/NC-exos are sufficient to inhibit angiogenesis by transferring miR-140-5p and targeting the Wnt/β-catenin pathway.

Exosomal miR-140-5p Expression of NP Is Negatively Correlated with Angiogenesis

To determine whether the level of exosomal miR-140-5p in NP tissues correlated with disc angiogenesis, NP tissues from IDD patients or idiopathic scoliosis were obtained and examined. Immunofluorescence staining showed that angiogenesis expression was higher in IDD than that of idiopathic scoliosis (Figure 7A), whereas the more NC-like cells were observed in H&E-stained NP tissues from idiopathic scoliosis patients (Figure 7B). Then, exosomes from the NP tissue-cultured medium were isolated, and the exosomal miR-140-5p expression was examined (Figure 7C). RT-PCR analysis showed that miR-140-3p from NP tissue-derived exosomes was downregulated in IDD patients (Figure 7D). Statistical analysis showed miR-140-5p levels and angiogenesis levels were negatively correlated (Figure 7E), indicating that downregulation of miR-25-3p in NP tissues

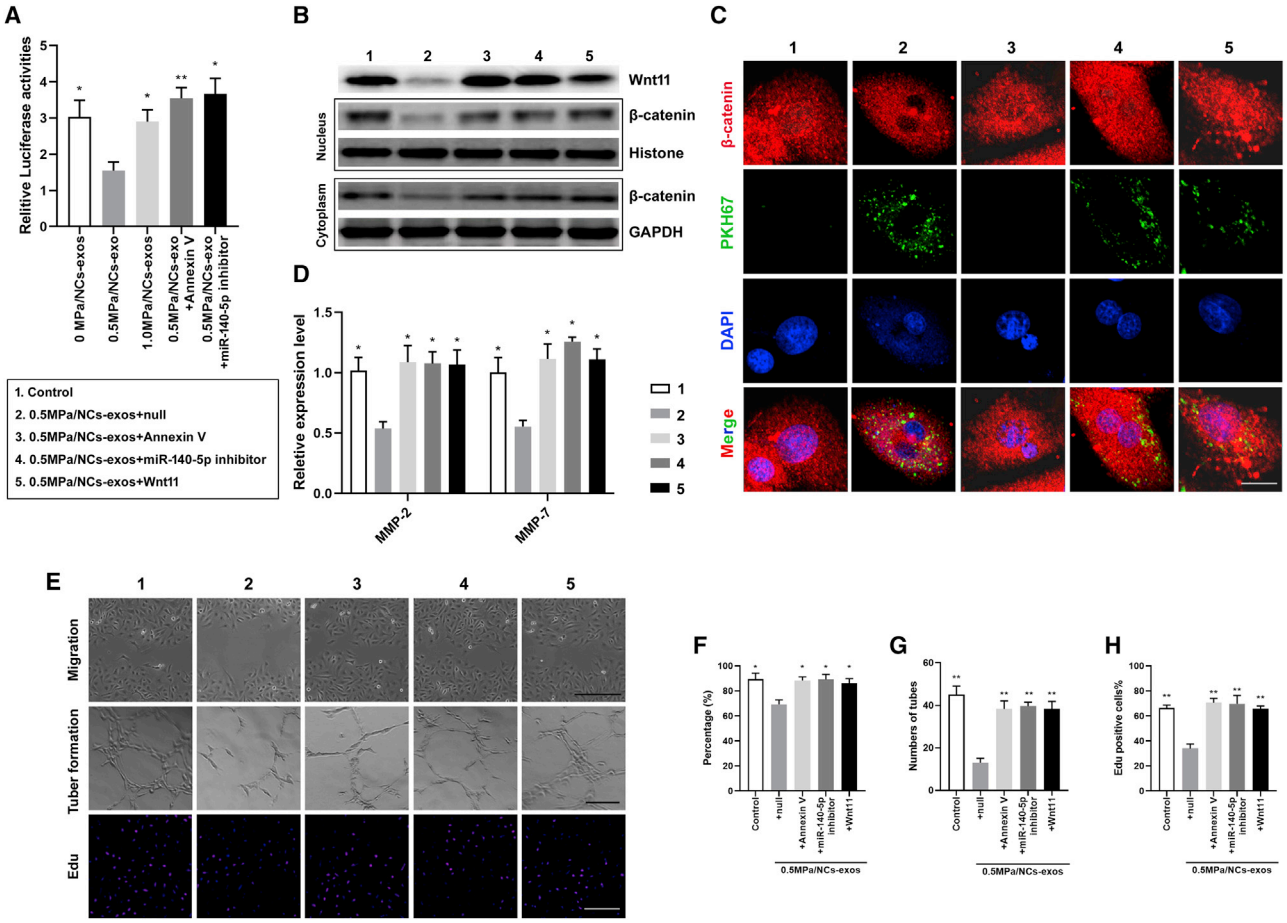

Figure 6. 0.5 MPa/NC-Exos Silence Wnt11 and Inhibit Angiogenesis in HUVECs

(A) Luciferase activities of 3′ UTR WNT11-luc constructs in HUVECs after incubation with 0 MPa/NC-exos, 0.5 MPa/NC-exos, 1.0 MPa/NC-exos, 0.5 MPa/NC-exos + Annexin V, and 0.5 MPa/NC-exos + miR-140-5p inhibitor. Mean ± SEM is provided (n = 3). *p < 0.05, **p < 0.01 for comparison with the 0.5-MPa/NC-exos group. (B) Western blotting analysis of Wnt11, β-catenin of nucleus/cytoplasm in HUVECs after incubation with 0.5 MPa/NC-exos, 0.5 MPa/NC-exos + Annexin V, 0.5 MPa/NC-exos + miR-140-5p inhibitor, and 0.5 MPa/NC-exos + Wnt11. (C) Immunofluorescence staining analysis of β-catenin and PKH67 lipid dye of HUVECs after incubation with 0.5 MPa/NC-exos, 0.5 MPa/NC-exos + Annexin V, 0.5 MPa/NC-exos + miR-140-5p inhibitor, and 0.5 MPa/NC-exos + Wnt11. β-catenin expression was decreased in the nucleus of the 0.5-MPa/NC-exos group. Bar, 10 μm. (D) ELISA detection of MMP-2 and MMP-7 levels in medium of HUVECs incubated with 0.5 MPa/NC-exos, 0.5 MPa/NC-exos + Annexin V, 0.5 MPa/NC-exos + miR-140-5p inhibitor, and 0.5 MPa/NC-exos + Wnt11. Mean ± SEM is provided (n = 3). *p < 0.05, **p < 0.01 for comparison with the 0.5-MPa/NC-exos group. (E–H) Migration (E and F), tube formation (E and G), and proliferation of HUVECs (E and H) after incubation with 0.5 MPa/NC-exos, 0.5 MPa/NC-exos + Annexin V, 0.5 MPa/NC-exos + miR-140-5p inhibitor, and 0.5 MPa/NC-exos + Wnt11. Bar, 100 μm. Mean ± SEM is provided (n = 3). *p < 0.05, **p < 0.01 for comparison with the 0.5-MPa/NC-exos group.

may contribute to elevated angiogenesis. These data suggest that the decreased expression of miR-140-5p from NP exosome is associated with disc angiogenesis.

0.5. MPa/NC-Exos Reduce Vascularization in Degenerated Disc Tissue

The effect of 0.5 MPa/NC-exos on disc vascularization was finally determined in an IDD animal model. As shown in Figures 8A and 8B, the application of 0.5 MPa/NC-exos in disc NP tissue showed decreased CD34 expression, indicating its anti-angiogenesis effect *in vivo*. Additionally, the degree of disc degeneration was evaluated by the disc height index (DHI), which was obtained from the micro-computed tomography (CT) evaluation. As shown in Figures 8C and 8D, the DHI stayed unchanged in the control group, whereas DHI decreased continuously in the IDD group after the operation. The treatment of 0.5 MPa/NC-exos increased the DHI significantly compared to the IDD group at week 6. These results indicate that 0.5 MPa/NC-exos exert therapeutical impact on the degenerated disc with an anti-angiogenesis effect *in vivo*.

DISCUSSION

NCs are large cells derived from the axial notochord in the embryonic period. They are characterized by containing giant cytoplasmic vacuoles. In some species, such as the canine and the rat, NCs exist within

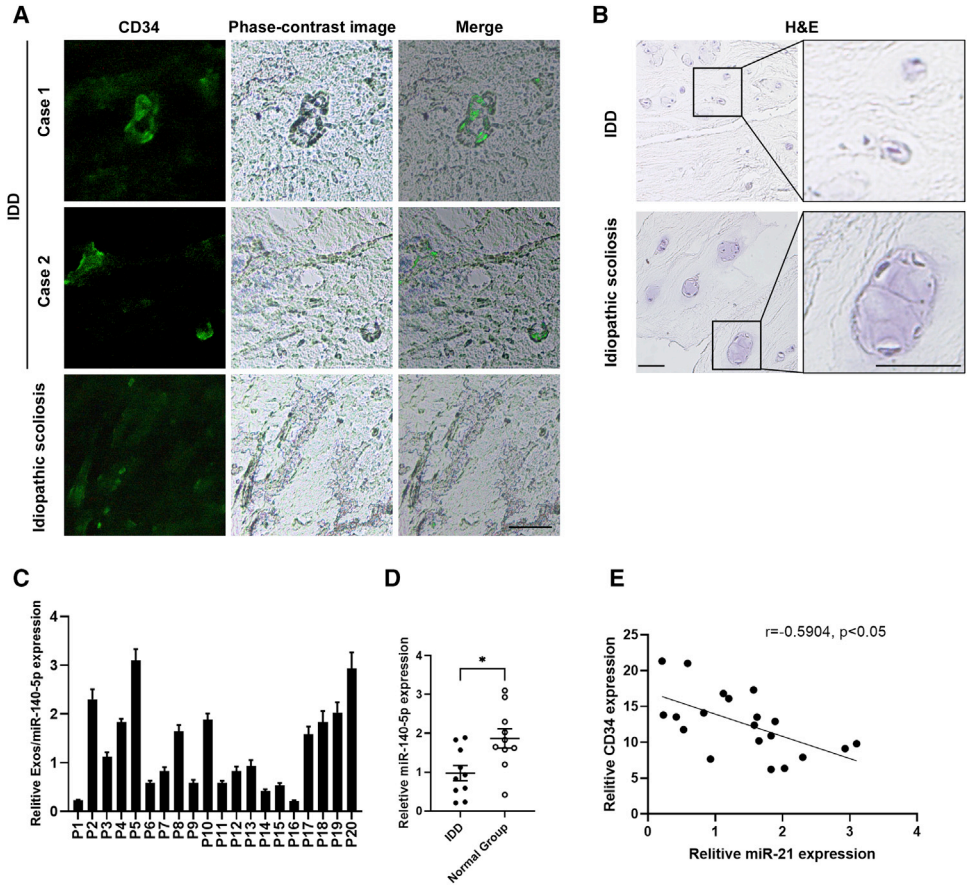

Figure 7. Exosomal miR-140-5p Expression of NP Is Negatively Associated with Disc Angiogenesis

(A) Immunofluorescence staining of CD34 in NP tissues from intervertebral disc degeneration (IDD) and idiopathic scoliosis patients. Bar, 100 μm. (B) H&E staining of NC-like cells in NP tissues from IDD and idiopathic scoliosis patients. Bars, 50 μm. (C) RT-PCR analysis of exosomal miR-140-5p expression of NP tissues from 20 cases. (D) RT-PCR analysis of exosomal miR-140-5p expression of NP tissues from IDD and idiopathic scoliosis patients. Mean ± SEM is provided. *$p < 0.05$. (E) Correlation analysis of miR-140-5p expression and CD34 expression. Pearson's correlation coefficient ($r = -0.5904$) and p value ($p < 0.05$) are shown.

the NP throughout most of their life, and these species demonstrate significantly postponed IDD. In humans, most NCs were proven to transform into chondrocyte-like NPs during adolescent life. It is speculated that early IDD happens with the disappearance of NCs in humans.[16] Previous evidence has been shown that the NCs play an important role in disc function via multiple ways, including activating degenerated NPs, stimulating chondrogenic differentiation, reducing native cell death, and inhibiting vascularization via secreting numerous biofactors.[7–9,17] However, it still remains unclear as to the mechanism of NC function.

In the current study, we unveiled that NC-exos could be secreted by NCs and internalized by endothelial cells. Then, we found that miR-140-5p could be delivered to endothelial cells via NC-exos with 0.5 MPa compressive load inducement, leading to angiogenesis inhibition, consequently contributing to intervertebral disc avascular status. We then showed that the level of exosomal miR-140-5p in NP tissue is negatively associated with angiogenesis in IDD. Furthermore, we demonstrated that 0.5 MPa/NC-exos could alleviate vascularization in an IDD animal model. Collectively, our study reveals the role of 0.5 MPa/NC-exo-derived miR-25-3p in anti-angiogenesis and its therapeutic potential for IDD.

Exosome-derived miRNAs can be transferred from various types of cells to endothelial cells and exert an efficient silencing effect on mRNAs to reprogram transcriptome. Numerous studies have shown that exosome-mediated transfer of miRNA to vascular epithelial cells involves an angiogenesis regulation.[18,19] In the intervertebral disc, we previously showed the important role of Fas ligand (FasL) in avascular maintenance.[3] We further elucidate the immune privilege of the disc, which is established by physical and molecular barriers, such as blood-NP barrier (BNB) and FasL.[4] Although the role of NCs or the NC-derived matrix in angiogenesis remains controversial,[20] studies have shown that NC-derived factors can inhibit angiogenic processes, indicating their potential role in inhibiting vascular in-growth treatment.[9] With the use of mass spectrometry, Matta

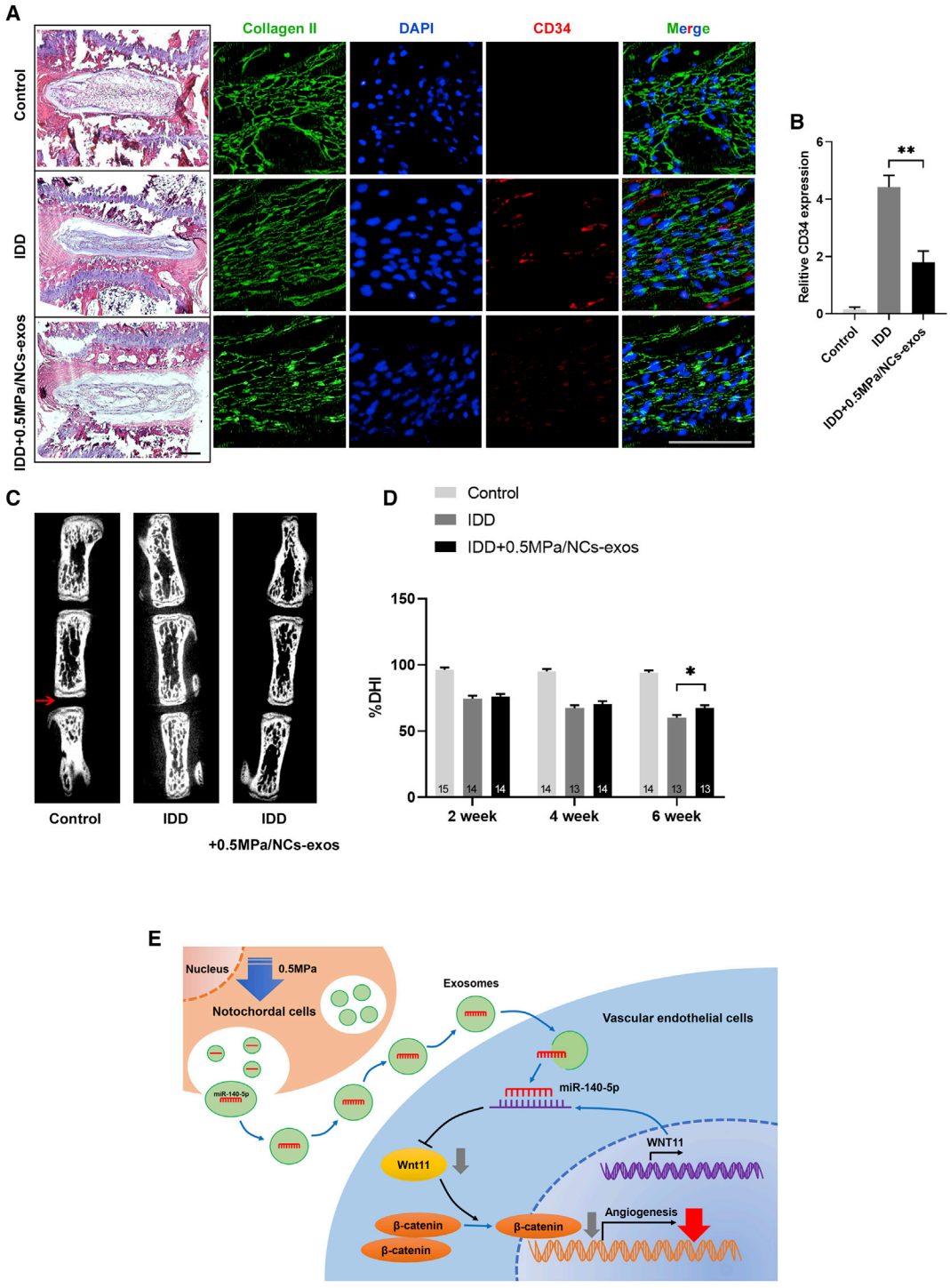

Figure 8. 0.5 MPa/NC-Exos Reduce Vascularization of Degenerated Disc Tissue

(A) Representative H&E staining of intervertebral disc and immunofluorescence staining of CD34 from the groups at 6 weeks. Bar, 100 μm. (B) Quantitative examination of CD34 expression in the immunofluorescence analysis. Mean ± SEM is provided (n = 5). **p < 0.01. (C) Representative micro-CT images of control group, IDD group, and IDD + 0.5 MPa/NC-exos group at 6 weeks. (D) %DHI of each group at 2, 4, and 6 weeks after the operation. Mean ± SEM is provided. The sample number for each group is indicated at the base of the corresponding bar. (E) Schematic of 0.5 MPa/NC-exos inhibits angiogenesis via the miR-140-5p/Wnt/β-catenin axis.

et al.[21] revealed transforming growth factor (TGF)-β1 and connective tissue growth factor (CTGF) as major hubs in protein-interaction networks of NC-derived conditioned medium. Nevertheless, the identification of key biofactors secreted by NCs that delay the onset of IDD is still in an early stage. In the current study, we, for the first time, showed the existence of NPs-exos and demonstrated that NC-exos produced with 0.5 MPa stimulation could inhibit disc angiogenesis by transferring miR-140-5p to endothelial cells. These data suggest the essential role of NC-exos in disc avascular maintenance.

Mechanical stress is of critical importance given the timely mechanical environment of the disc. Studies have indicated the close relationship of the disc with biomechanics.[22] Previously, we found that compressive load cultures could induce CK8 phosphorylation and downregulation in NPs.[23] As for the NCs, Saggese et al.[24] showed that NCs are more resistant to mechanical stresses compared to NPs, indicating their potential role in compression loaded disc. In the early stage of spine development, NCs are squeezed into the disc by the pushing force derived from the forming vertebrae, leading the NCs into a specific physiological environment with compressed mechanical force. On the other hand, it is also shown that high mechanical force could lead to the exhaustion of NC resources.[25,26] These studies suggest that a particular range of mechanical stresses is necessary for normal NC survival and function. Here, we found that 0.5 MPa was able to simulate the miR-140-5p package in NC-exos with no influence on NC viability, indicating that 0.5 MPa might be a suitable mechanical ambient for modulating NC function.

miR-140-5p has been shown to be involved in cell migration, proliferation, and metastasis.[27–29] Meanwhile, the Wnt signaling pathway is critically involved in angiogenesis through the modulation of endothelial cell proliferation, migration, vascular sprouting, and vascular system maturation.[30,31] Importantly, β-catenin regulation was regarded as one of the most important downstream pathways of Wnt-dependent signaling.[32,33] In the intervertebral disc, however, their roles in angiogenesis have not been elucidated. Here, we showed that miR-140-5p is upregulated in NC-exos cultured in a 0.5-MPa compressive load, and miR-140-5p transferred by these NC-exos inhibited angiogenesis in vascular endothelial cells. Wnt11 and downstream β-catenin signaling were shown to be the functional targets. Wnt11 is one of the Wnt family members and works almost exclusively through noncanonical signaling mechanisms. Studies have revealed that Wnt11 stimulates proliferation, migration, and invasion of many types of cells by activating β-catenin and inducing its nuclear accumulation.[34,35] Additionally, Wnt11 was shown to be involved in the regulation of MMP expression.[36] The current study provides evidence that NC-exo-derived miR-140-5p inhibits the secretion of MMP-2 and MMP-7 in endothelial cells. MMPs are a family of zinc-containing and zinc-dependent enzymes, which have been shown to facilitate blood vessel infiltration by inducing degradation of the extracellular matrix.[37] This result suggests that the exosomal miR-140-5p could reduce the invasive ability of blood vessels by inhibiting MMP expression. Collectively, our data showed that NCs might exhibit their anti-angiogenesis ability via NC-exo-derived miR-140-5p.

Studies have suggested that humans retain a small proportion of NCs, typically less than 20% of the total NP cell population into adulthood.[38,39] We have previously shown that the CK8-positive cells exist in adult human NP tissues and decrease with IDD degree, suggesting the existence of the remaining NCs.[40] In this study, we demonstrated that the expression of miR-140-3p from NP tissue-derived exosomes was negatively correlated angiogenesis levels in human NP tissues. These data indicate that the exosomal miR-140-5p might be produced by the remaining NCs and suggest their potential role in normal disc function maintenance.

Recent studies have revealed the emerging therapeutical role of exosomes derived from MSCs.[41] In the intervertebral disc, MSC-derived exosomes were proven to ameliorate IDD via transferring various biofactors and regulating the corresponding downstream pathways.[42–44] However, there is a paucity of information in the literature pertaining to the existence of NC-exos and their impact on IDD. To examine the *in vivo* effect of NC-exos, we further applied the NC-exos in an IDD animal model. We found that 0.5 MPa/NC-exos could reduce the vascularization of degenerated disc tissue. Moreover, IDD progress was alleviated in the micro-CT measurement. This observation was consistent with the *in vitro* study and indicated that NC-exos might be used as a potential option for further IDD treatment.

In conclusion, our findings showed that the 0.5 MPa/NC-exos inhibit angiogenesis via regulating the miR-140-5p/Wnt/β-catenin axis in vascular epithelial cells, providing insights into the anti-angiogenesis mechanism of NCs. Consequently, the current study increases our understanding of the therapeutic potential of NCs for IDD.

MATERIALS AND METHODS

NC Isolation and Culture

Forty adult male Sprague-Dawley rats, weighing 200–220 g, were obtained from the Experimental Animal Center of Fourth Military Medical University. All animal procedures were performed under the approval and guidance of the Institutional Ethics Review Board of Xijing Hospital. NCs were obtained following the protocol described previously (Figure 1A).[45] Briefly, following the application of intravenous general anesthesia, the rats were sacrificed, and the lumbar NP tissue was harvested from each disc. The NP tissues were then washed with phosphate-buffered saline (PBS) and digested for 40 min in 0.2% pronase (Gibco-BRL, Carlsbad, CA, USA) (0.005 mL/mg of tissue). After being washed twice, the tissues were then incubated in 0.25% type II collagenase (Gibco-BRL, Carlsbad, CA, USA) (0.002 mL/mg of tissue) at 37°C under gentle agitation for 4 h. Then, the tissue debris was detached by a 70-μm pore-size nylon mesh. It has been shown that NCs did not adhere to the flask until day 6; thus, these cells were separated from the chondrocyte-like NPs on day 3. The NCs were then isolated by a serial filtration procedure with a mesh diameter of 40, 25, and 15 μm. The yielded NCs are approximately 100 cells/mg tissue, and NPs are approximately 200 cells/mg tissue. NCs were seeded in culture flasks with DMEM/F12-based medium containing 10% exosome-free fetal bovine serum (Thermo Fisher

Scientific, Waltham, MA, USA). The culture flasks were then placed in incubator with 20% oxygen and 5% CO_2 at 37°C.

NC-Exos Isolation and Identification

NC-exos were isolated as described previously.[19,46] Briefly, cell culture medium was collected and centrifuged at 200 × *g* for 10 min and 10,000 × *g* for 30 min to remove cells and dead cells. Then, supernatant was obtained and filtered through 0.22 μm membrane filters with pressure to remove particles larger than 0.22 μm in diameter. After ultracentrifugation at 100,000 × *g* for 80 min at 4°C, the exosomes were pelleted. Then, the pellets were washed and resuspended in PBS (Figure 2A). For observation of exosome morphology, the morphology of the exosomes was observed by TEM (JSM-4800; Hitachi, Japan). For size distribution assay, the exosomes were resuspended in PBS and measured by nanoparticle trafficking analysis (NTA) using the NanoSight NS300 system (Malvern, UK), according to the manufacturer's instructions. The exosomes were quantified by the Bradford protein assay and stored at −80°C for further use. For exosomes from NP tissues, NP tissues were incubated in the serum-free culture media at 37°C in a humidified 5% CO_2 incubator for 6 h. The media were subjected to the mentioned procedures. The exosomes were obtained and managed under schemes according to the corresponding procedures.

Compressive Load Culture

The compressive load culture was established according to our previous studies.[23,47] The culture system consisted of a compression culture chamber and gas cylinder. To provide compressive stress, the culture chamber was linked with a high-pressure gas cylinder. The samples were then subjected to controllable compressive stress at 0 MPa, 0.5 MPa, and 1.0 MPa for 24 and 48 h (Figure 2I).

Internalization of NC-Exos by HUEVCs

NC-exos were labeled with PKH67 (Sigma-Aldrich), according to the manufacturer's instructions. Briefly, 250 μg of NC-exos was mixed with PKH67 in 1 mL of diluent C (Sigma-Aldrich) with a final concentration of 2×10^{-6} M PKH67. Then, 2 mL of 5% BSA/PBS was added for neutralization after 5 min incubation. The NC-exos were then washed by PBS and incubated with HUVECs. After 6 h, HUVECs were observed by fluorescence confocal microscope (Nikon, Tokyo, Japan) and examined by flow cytometry. Additionally, NCs were transfected with Cy3-labeled miR-140-5p mimics and cultured in compressive loads with 0 MPa, 0.5 MPa, and 1.0 MPa. The NC-exos were labeled by PKH67 and incubated with HUVECs. 4′,6-diamidino-2-phenylindole (DAPI) was used for cellular nuclei staining. Imaging of exosome uptake was performed by fluorescence confocal microscope.

Migration Assay, Angiogenesis Assay, and 5-Ethynyl-2′-Deoxyuridine (EdU) Assay

Migration was measured by scratching the HUVEC confluent layer in a 24-well plate with a P200 pipette tip. Then, PBS was used to wash the loose cells. For each group, 300 μL of test medium was applied, and the plate was incubated at 37°C. HUVEC migration was quantified and monitored. For further evaluation, the images were processed by WimScratch (Wound Healing Assay Image Analysis). Cells from three random fields were counted. Tube formation assay was performed as follows: Matrigel matrix (Corning) was used to plate in a 24-well plate. The plates were incubated at 37°C for 30 min, and HUVECs were seeded on the Matrigel-coated wells. The plate was then incubated at 37°C in a 5% CO_2 humidified atmosphere. Tube formation was observed with a microscope. The number of tubes was measured for tube formation ability. For EdU assay, EdU Staining Proliferation Kit (Abcam) was used. Briefly, 100 μl EdU solution was added into a 96-well plate for 2 h incubation. Then, fixative solution was added and incubated for 15 min. After being washed with PBS, the cells were incubated in permeabilization buffer for 20 min. Then, reaction mix to fluorescently label EdU was added. After 30 min, the wells were viewed and photographed using a confocal fluorescence microscope. The EdU-positive rate was counted as positive cells/overall cells × 100%. For each sample, the cell number was counted at least three times.

miRNA Microarray Analysis

Total RNA from NC-exos was extracted by Trizol (Tiangen, Beijing) and assessed by an Agilent 2100 BioAnalyzer (Agilent Technologies, Santa Clara, CA, USA) and Qubit Fluorometer (Invitrogen). Sequence libraries were generated and sequenced by CapitalBio Technology (Beijing, China) using NEB Next Multiplex Small RNA Library Prep Set for Illumina (NEB, USA) following the manufacturer's instructions. PCR amplification was performed using LongAmp Taq 2X Master Mix, SR Primer for Illumina, and Index (X) Primer. Library quality was assessed on the Agilent Bioanalyzer 2100 system using DNA High Sensitivity Chips. The library preparations were sequenced on an Illumina HiSeq 2500 platform following the manufacturer's instructions. A p value of 0.05 and (log2[fold change]) >1 were set as thresholds for significantly differential expression.

Nuclear and Cytoplasm Fractionation

Nuclear and cytoplasm fractionation was conducted using the Nuclear and Cytoplasmic Extraction Reagents (Thermo Fisher Scientific), according to the manufacturer's instructions. Briefly, cells were harvested and washed once with cold PBS. Cells were then pelleted by 500 × *g* for 3 min. Ice-cold cytoplasmic extraction reagent (CER) I and CER II were added to the cell pellet. After being vortexed, cells were centrifuged at 15,000 × *g* at 4°C for 5 min. Supernatant was collected containing the cytoplasm fraction. The remaining cell debris was then suspended in nucleotide excision repair (NER), rotated at 4°C for 15 s, and repeated 3 times every 10 min. Cytoplasm and nuclear fractionation were stored at −80°C for further detection.

Western Blotting

Cell or exosome lysates were prepared in 3-(*N*-morpholino)propanesulfonic acid (MOPS) buffer on ice for 30 min. Then, debris was removed by centrifugation for 20 min at 4°C. Protein concentration was measured with the bicinchoninic acid (BCA) assay (Sigma, St. Louis, MO, USA). After being electrophoresed in 10% Bis-Tris gel, proteins were transferred to the polyvinylidene fluoride (PVDF)

membrane. The samples were then blocked in the nonspecific binding sites overnight. Following transfer to nitrocellulose membranes, samples were incubated with the primary antibodies as follows: rabbit anti-CK8 (1:200), rabbit anti-vimentin (1:200), rabbit anti-glyceraldehyde 3-phosphate dehydrogenase (GAPDH) (1:1,000), mouse monoclonal anti-CD63 (1:200), rabbit anti-Tsg101 (1:200), rabbit anti-calnexin (1:200), rabbit anti-Wnt11 (1:500), and rabbit anti-β catenin (1:500) (Abcam, Cambridge, MA, USA), Antibody labeling was identified using horseradish peroxidase (HRP)-conjugated secondary antibodies (Cell Signaling Technology, Boston, MA, USA). Images were analyzed by densitometry from Scion Image.

RT-PCR

Total RNA was extracted using the Total RNA Kit (Omega Biotek, Norcross, GA, USA) and normalized to a cell number before RT-PCR. Thereafter, RT-PCR was performed according to the manufacturer's instructions in a 7500 Real-Time PCR System (Applied Biosystems, Foster City, CA, USA) with SYBR Premix Ex Taq (TaKaRa). The sequences of primers are shown in Table S1. The PCR reaction was conducted using 25 mL of sample cDNA, 2.5 mL of 10 PCR buffer, 2.0 mL of $MgSO_4$ (25 mM), 2.5 mL deoxyribonucleotide triphosphate (dNTP) mix (2 mM), 0.5 mL Taq DNA Polymerase (2 U/mL), and 15.8 mL deionized H_2O. The reaction mixture was heated to 95°C for 2.5 min and then amplified for 40 cycles as follows: 95°C for 30 s (denaturation), 50°C for 30 s (annealing), and 65°C for 10 s (extension).

Enzyme-Linked Immunosorbent Assay (ELISA) Measurement

According to the manufacturer's instruction, ELISA kits (Abcam, Cambridge, MA, USA) were applied to detect the concentration of MMP-2 and MMP-7 in the HUVEC cultured medium. The concentration was determined in triplicate in each sample, and the average measurement was considered to be the final concentration.

Luciferase Activity Assay

A Wnt11 gene 3′ UTR segment was amplified using PCR and inserted into the vector. Lipofectamine 2000 (Invitrogen) was used to cotransfections of Wnt11 3′ UTR plasmids with miR-140-5p lentivirus vector into the cells. 48 h after transfection by the dual luciferase, luciferase activity was examined by the Reporter Assay System (Promega). All experiments were performed in triplicate, and each assay was repeated three times.

RNA Interference and Plasmids

Mimics and inhibitor of miR-140-5p were purchased from GenePharma. The sequences of miR-140-5p mimics and inhibitor were listed in Table S2. Lentivirus vectors expressing miR-140-5p were constructed and produced by GeneChem. In rescue experiments, cells that stably expressed miR-140-5p or incubated with exosomal miR-140-5p were transfected with Wnt11 expressing plasmids (GeneCopoeia). In the exosome transfection experiments, the miR-140-5p inhibitor (GenePharma) was loaded in NC-exos with the Exo-Fect Exosome Transfection Kit (System Biosciences), according to the manufacturer's instruction.

Human NP Tissue Collection

Human NP tissues and magnetic resonance imaging (MRI) data were obtained, as described previously.[23] Ethics approval was obtained from the Institutional Review Board of Xijing Hospital. Briefly, written, informed consents were collected from each patient. NP tissues were obtained from patients with idiopathic scoliosis (n = 10; average age 19.3 [range 16–24] years) and IDD (n = 10; average age 46.2 [range 34–68] years) as control and degenerative groups. Samples were obtained within 2 h after surgery. NP tissues were identified and separated by a stereotaxic microscope. Then, the NP tissues were cultured in DMEM/F12-based medium containing 10% exosome-free fetal bovine serum (Thermo Fisher Scientific, Waltham, MA, USA) for exosome isolation or frozen and stored in −80°C for further immunofluorescence.

Immunofluorescence

Cells or NP tissues were fixed in 4% paraformaldehyde for 10 min at room temperature. The samples were then washed with PBS and incubated with blocking buffer (1% BSA, 0.4% Triton X-100, and 4% normal serum in PBS) for 30 min. Thereafter, the samples were stained with primary antibodies and secondary antibodies (1:200; Abcam) for 1 h at room temperature. Thereafter, the cell nucleus was stained with DAPI solution (1:1,000; Invitrogen) for 1 min at room temperature. The immunostaining results were examined and photographed with a fluorescence microscope (Nikon, Tokyo, Japan). For quantitative examination, the immunostaining results of the animal specimens were analyzed by Image-Pro 6.0 software.

In Vivo Validation in IDD Animal Model

The IDD animal model was established as previously reported.[48] Briefly, a total of forty-five C57 mice, aged 10–12 weeks, were used. The mice were anesthetized with intraperitoneal injection of Hypnorm (0.5 mL/kg) and Dormicum (0.5 mL/kg). The tail skin of the mice was longitudinally incised, and the subcutaneous connective tissues were separated. C4/C5 discs were then punctured by a 31G needle through the AF at a controlled depth of needle bevel under microscopic guidance. Mice were returned to treatment 2 weeks after puncture surgery. C4/C5 discs were injected with 2 μL of 0.5 MPa/NC-exos. Micro-CT (eXplore Locus SP; GE Healthcare, Fairfield, CT, USA) was conducted for quantitative disc height evaluation. DHI was calculated as the percent of the disc height to the length of the adjacent vertebral body. Change of DHI was expressed as % DHI (postinjection DHI/preinjection DHI).

Statistical Analysis

The SPSS statistical package (SPSS, Chicago, IL, USA) was used for statistical analysis. Student's t test was used in the analysis of two-group parameters. ANOVA test was used in comparisons of multiple groups. A p value <0.05 was considered significant.

SUPPLEMENTAL INFORMATION

Supplemental Information can be found online at https://doi.org/10.1016/j.omtn.2020.10.021.

AUTHOR CONTRIBUTIONS

Z.-J.L. and Z.S. designed the research and wrote the manuscript. Z.S., B.L., Z.-H.L., J.F., D.W., and Z.X. performed the experiments. W.S., B.-Y.C., and D.G. provided assistance and guidance on experiments. All authors read and approved the final version.

CONFLICTS OF INTEREST

The authors declare no competing interests.

ACKNOWLEDGMENTS

This work was supported by grants from the Shaanxi Natural Science Foundation (2020JM-319); National Natural Science Foundation of China (82002348); Key Project of National Natural Science Foundation of China (81730065); and Natural Science Foundation of Xijing Hospital (XJZT18MJ17).

REFERENCES

1. Liu, Z.H., Sun, Z., Wang, H.Q., Ge, J., Jiang, T.S., Chen, Y.F., Ma, Y., Wang, C., Hu, S., Samartzis, D., and Luo, Z.J. (2013). FasL expression on human nucleus pulposus cells contributes to the immune privilege of intervertebral disc by interacting with immunocytes. Int. J. Med. Sci. *10*, 1053–1060.

2. Sun, Z., Liu, Z.H., Chen, Y.F., Zhang, Y.Z., Wan, Z.Y., Zhang, W.L., Che, L., Liu, X., Wang, H.Q., and Luo, Z.J. (2013). Molecular immunotherapy might shed a light on the treatment strategies for disc degeneration and herniation. Med. Hypotheses *81*, 477–480.

3. Sun, Z., Wan, Z.Y., Guo, Y.S., Wang, H.Q., and Luo, Z.J. (2013). FasL on human nucleus pulposus cells prevents angiogenesis in the disc by inducing Fas-mediated apoptosis of vascular endothelial cells. Int. J. Clin. Exp. Pathol. *6*, 2376–2385.

4. Sun, Z., Liu, B., and Luo, Z.J. (2020). The Immune Privilege of the Intervertebral Disc: Implications for Intervertebral Disc Degeneration Treatment. Int. J. Med. Sci. *17*, 685–692.

5. Rodrigues-Pinto, R., Ward, L., Humphreys, M., Zeef, L.A.H., Berry, A., Hanley, K.P., Hanley, N., Richardson, S.M., and Hoyland, J.A. (2018). Human notochordal cell transcriptome unveils potential regulators of cell function in the developing intervertebral disc. Sci. Rep. *8*, 12866.

6. Bach, F.C., Tellegen, A.R., Beukers, M., Miranda-Bedate, A., Teunissen, M., de Jong, W.A.M., de Vries, S.A.H., Creemers, L.B., Benz, K., Meij, B.P., et al. (2018). Biologic canine and human intervertebral disc repair by notochordal cell-derived matrix: from bench towards bedside. Oncotarget *9*, 26507–26526.

7. Bai, X.D., Li, X.C., Chen, J.H., Guo, Z.M., Hou, L.S., Wang, D.L., He, Q., and Ruan, D.K. (2017). * Coculture with Partial Digestion Notochordal Cell-Rich Nucleus Pulposus Tissue Activates Degenerative Human Nucleus Pulposus Cells. Tissue Eng. Part A *23*, 837–846.

8. de Vries, S.A., Potier, E., van Doeselaar, M., Meij, B.P., Tryfonidou, M.A., and Ito, K. (2015). Conditioned medium derived from notochordal cell-rich nucleus pulposus tissue stimulates matrix production by canine nucleus pulposus cells and bone marrow-derived stromal cells. Tissue Eng. Part A *21*, 1077–1084.

9. Cornejo, M.C., Cho, S.K., Giannarelli, C., Iatridis, J.C., and Purmessur, D. (2015). Soluble factors from the notochordal-rich intervertebral disc inhibit endothelial cell invasion and vessel formation in the presence and absence of pro-inflammatory cytokines. Osteoarthritis Cartilage *23*, 487–496.

10. Dreyer, F., and Baur, A. (2016). Biogenesis and Functions of Exosomes and Extracellular Vesicles. Methods Mol. Biol. *1448*, 201–216.

11. Wolfers, J., Lozier, A., Raposo, G., Regnault, A., Théry, C., Masurier, C., Flament, C., Pouzieux, S., Faure, F., Tursz, T., et al. (2001). Tumor-derived exosomes are a source of shared tumor rejection antigens for CTL cross-priming. Nat. Med. *7*, 297–303.

12. Lema, D.A., and Burlingham, W.J. (2019). Role of exosomes in tumour and transplant immune regulation. Scand. J. Immunol. *90*, e12807.

13. Asghar, S., Litherland, G.J., Lockhart, J.C., Goodyear, C.S., and Crilly, A. (2020). Exosomes in intercellular communication and implications for osteoarthritis. Rheumatology (Oxford) *59*, 57–68.

14. Li, L., Li, C., Wang, S., Wang, Z., Jiang, J., Wang, W., Li, X., Chen, J., Liu, K., Li, C., and Zhu, G. (2016). Exosomes Derived from Hypoxic Oral Squamous Cell Carcinoma Cells Deliver miR-21 to Normoxic Cells to Elicit a Prometastatic Phenotype. Cancer Res. *76*, 1770–1780.

15. Wang, F., Gao, Z.X., Cai, F., Sinkemani, A., Xie, Z.Y., Shi, R., Wei, J.N., and Wu, X.T. (2017). Formation, function, and exhaustion of notochordal cytoplasmic vacuoles within intervertebral disc: current understanding and speculation. Oncotarget *8*, 57800–57812.

16. Risbud, M.V., and Shapiro, I.M. (2011). Notochordal cells in the adult intervertebral disc: new perspective on an old question. Crit. Rev. Eukaryot. Gene Expr. *21*, 29–41.

17. Mehrkens, A., Matta, A., Karim, M.Z., Kim, S., Fehlings, M.G., Schaeren, S., and Mark Erwin, W. (2017). Notochordal cell-derived conditioned medium protects human nucleus pulposus cells from stress-induced apoptosis. Spine J. *17*, 579–588.

18. Sun, Z., Shi, K., Yang, S., Liu, J., Zhou, Q., Wang, G., Song, J., Li, Z., Zhang, Z., and Yuan, W. (2018). Effect of exosomal miRNA on cancer biology and clinical applications. Mol. Cancer *17*, 147.

19. Zeng, Z., Li, Y., Pan, Y., Lan, X., Song, F., Sun, J., Zhou, K., Liu, X., Ren, X., Wang, F., et al. (2018). Cancer-derived exosomal miR-25-3p promotes pre-metastatic niche formation by inducing vascular permeability and angiogenesis. Nat. Commun. *9*, 5395.

20. de Vries, S.A.H., van Doeselaar, M., Meij, B.P., Tryfonidou, M.A., and Ito, K. (2018). Notochordal cell matrix: An inhibitor of neurite and blood vessel growth? J. Orthop. Res. *36*, 3188–3195.

21. Matta, A., Karim, M.Z., Isenman, D.E., and Erwin, W.M. (2017). Molecular Therapy for Degenerative Disc Disease: Clues from Secretome Analysis of the Notochordal Cell-Rich Nucleus Pulposus. Sci. Rep. *7*, 45623.

22. Vergroesen, P.P., Kingma, I., Emanuel, K.S., Hoogendoorn, R.J., Welting, T.J., van Royen, B.J., van Dieën, J.H., and Smit, T.H. (2015). Mechanics and biology in intervertebral disc degeneration: a vicious circle. Osteoarthritis Cartilage *23*, 1057–1070.

23. Sun, Z., Guo, Y.S., Yan, S.J., Wan, Z.Y., Gao, B., Wang, L., Liu, Z.H., Gao, Y., Samartzis, D., Lan, L.F., et al. (2013). CK8 phosphorylation induced by compressive loads underlies the downregulation of CK8 in human disc degeneration by activating protein kinase C. Lab. Invest. *93*, 1323–1330.

24. Saggese, T., Thambyah, A., Wade, K., and McGlashan, S.R. (2020). Differential Response of Bovine Mature Nucleus Pulposus and Notochordal Cells to Hydrostatic Pressure and Glucose Restriction. Cartilage *11*, 221–233.

25. Hong, X., Zhang, C., Wang, F., and Wu, X.T. (2018). Large Cytoplasmic Vacuoles within Notochordal Nucleus Pulposus Cells: A Possible Regulator of Intracellular Pressure That Shapes the Cytoskeleton and Controls Proliferation. Cells Tissues Organs *206*, 9–15.

26. Yurube, T., Hirata, H., Kakutani, K., Maeno, K., Takada, T., Zhang, Z., Takayama, K., Matsushita, T., Kuroda, R., Kurosaka, M., and Nishida, K. (2014). Notochordal cell disappearance and modes of apoptotic cell death in a rat tail static compression-induced disc degeneration model. Arthritis Res. Ther. *16*, R31.

27. Rothman, A.M., Arnold, N.D., Pickworth, J.A., Iremonger, J., Ciuclan, L., Allen, R.M., Guth-Gundel, S., Southwood, M., Morrell, N.W., Thomas, M., et al. (2016). MicroRNA-140-5p and SMURF1 regulate pulmonary arterial hypertension. J. Clin. Invest. *126*, 2495–2508.

28. Fang, Z., Yin, S., Sun, R., Zhang, S., Fu, M., Wu, Y., Zhang, T., Khaliq, J., and Li, Y. (2017). miR-140-5p suppresses the proliferation, migration and invasion of gastric cancer by regulating YES1. Mol. Cancer *16*, 139.

29. Lan, H., Chen, W., He, G., and Yang, S. (2015). miR-140-5p inhibits ovarian cancer growth partially by repression of PDGFRA. Biomed. Pharmacother. *75*, 117–122.

30. Zhang, Q., Lou, Y., Zhang, J., Fu, Q., Wei, T., Sun, X., Chen, Q., Yang, J., Bai, X., and Liang, T. (2017). Hypoxia-inducible factor-2α promotes tumor progression and has crosstalk with Wnt/β-catenin signaling in pancreatic cancer. Mol. Cancer *16*, 119.

31. Hübner, K., Cabochette, P., Diéguez-Hurtado, R., Wiesner, C., Wakayama, Y., Grassme, K.S., Hubert, M., Guenther, S., Belting, H.G., Affolter, M., et al. (2018). Wnt/β-catenin signaling regulates VE-cadherin-mediated anastomosis of brain capillaries by counteracting S1pr1 signaling. Nat. Commun. *9*, 4860.

32. Perugorria, M.J., Olaizola, P., Labiano, I., Esparza-Baquer, A., Marzioni, M., Marin, J.J.G., Bujanda, L., and Banales, J.M. (2019). Wnt-β-catenin signalling in liver development, health and disease. Nat. Rev. Gastroenterol. Hepatol. *16*, 121–136.

33. Schaefer, K.N., and Peifer, M. (2019). Wnt/Beta-Catenin Signaling Regulation and a Role for Biomolecular Condensates. Dev. Cell *48*, 429–444.

34. Stefater, J.A., 3rd, Lewkowich, I., Rao, S., Mariggi, G., Carpenter, A.C., Burr, A.R., Fan, J., Ajima, R., Molkentin, J.D., Williams, B.O., et al. (2011). Regulation of angiogenesis by a non-canonical Wnt-Flt1 pathway in myeloid cells. Nature *474*, 511–515.

35. Franco, C.A., Jones, M.L., Bernabeu, M.O., Vion, A.C., Barbacena, P., Fan, J., Mathivet, T., Fonseca, C.G., Ragab, A., Yamaguchi, T.P., et al. (2016). Non-canonical Wnt signalling modulates the endothelial shear stress flow sensor in vascular remodelling. eLife *5*, e07727.

36. Mori, H., Yao, Y., Learman, B.S., Kurozumi, K., Ishida, J., Ramakrishnan, S.K., Overmyer, K.A., Xue, X., Cawthorn, W.P., Reid, M.A., et al. (2016). Induction of WNT11 by hypoxia and hypoxia-inducible factor-1α regulates cell proliferation, migration and invasion. Sci. Rep. *6*, 21520.

37. Liu, Y., Zhang, H., Yan, L., Du, W., Zhang, M., Chen, H., Zhang, L., Li, G., Li, J., Dong, Y., and Zhu, D. (2018). MMP-2 and MMP-9 contribute to the angiogenic effect produced by hypoxia/15-HETE in pulmonary endothelial cells. J. Mol. Cell. Cardiol. *121*, 36–50.

38. Stosiek, P., Kasper, M., and Karsten, U. (1988). Expression of cytokeratin and vimentin in nucleus pulposus cells. Differentiation *39*, 78–81.

39. Weiler, C., Nerlich, A.G., Schaaf, R., Bachmeier, B.E., Wuertz, K., and Boos, N. (2010). Immunohistochemical identification of notochordal markers in cells in the aging human lumbar intervertebral disc. Eur. Spine J. *19*, 1761–1770.

40. Sun, Z., Wang, H.Q., Liu, Z.H., Chang, L., Chen, Y.F., Zhang, Y.Z., Zhang, W.L., Gao, Y., Wan, Z.Y., Che, L., et al. (2013). Down-regulated CK8 expression in human intervertebral disc degeneration. Int. J. Med. Sci. *10*, 948–956.

41. Joo, H.S., Suh, J.H., Lee, H.J., Bang, E.S., and Lee, J.M. (2020). Current Knowledge and Future Perspectives on Mesenchymal Stem Cell-Derived Exosomes as a New Therapeutic Agent. Int. J. Mol. Sci. *21*, 727.

42. Liao, Z., Luo, R., Li, G., Song, Y., Zhan, S., Zhao, K., Hua, W., Zhang, Y., Wu, X., and Yang, C. (2019). Exosomes from mesenchymal stem cells modulate endoplasmic reticulum stress to protect against nucleus pulposus cell death and ameliorate intervertebral disc degeneration in vivo. Theranostics *9*, 4084–4100.

43. Xia, C., Zeng, Z., Fang, B., Tao, M., Gu, C., Zheng, L., Wang, Y., Shi, Y., Fang, C., Mei, S., et al. (2019). Mesenchymal stem cell-derived exosomes ameliorate intervertebral disc degeneration via anti-oxidant and anti-inflammatory effects. Free Radic. Biol. Med. *143*, 1–15.

44. Zhu, L., Shi, Y., Liu, L., Wang, H., Shen, P., and Yang, H. (2020). Mesenchymal stem cells-derived exosomes ameliorate nucleus pulposus cells apoptosis via delivering miR-142-3p: therapeutic potential for intervertebral disc degenerative diseases. Cell Cycle *19*, 1727–1739.

45. Kim, J.H., Deasy, B.M., Seo, H.Y., Studer, R.K., Vo, N.V., Georgescu, H.I., Sowa, G.A., and Kang, J.D. (2009). Differentiation of intervertebral notochordal cells through live automated cell imaging system in vitro. Spine *34*, 2486–2493.

46. Lu, K., Li, H.Y., Yang, K., Wu, J.L., Cai, X.W., Zhou, Y., and Li, C.Q. (2017). Exosomes as potential alternatives to stem cell therapy for intervertebral disc degeneration: in-vitro study on exosomes in interaction of nucleus pulposus cells and bone marrow mesenchymal stem cells. Stem Cell Res. Ther. *8*, 108.

47. Sun, Z., Luo, B., Liu, Z.H., Samartzis, D., Liu, Z., Gao, B., Huang, L., and Luo, Z.J. (2015). Adipose-derived stromal cells protect intervertebral disc cells in compression: implications for stem cell regenerative disc therapy. Int. J. Biol. Sci. *11*, 133–143.

48. Sun, Z., Luo, B., Liu, Z., Huang, L., Liu, B., Ma, T., Gao, B., Liu, Z.H., Chen, Y.F., Huang, J.H., and Luo, Z. (2016). Effect of perfluorotributylamine-enriched alginate on nucleus pulposus cell: Implications for intervertebral disc regeneration. Biomaterials *82*, 34–47.

OMTN, Volume 22

Supplemental Information

Notochordal-Cell-Derived Exosomes Induced by Compressive Load Inhibit Angiogenesis via the miR-140-5p/Wnt/β-Catenin Axis

Zhen Sun, Bing Liu, Zhi-Heng Liu, Wen Song, Dong Wang, Bei-Yu Chen, Jing Fan, Zhe Xu, Dan Geng, and Zhuo-Jing Luo

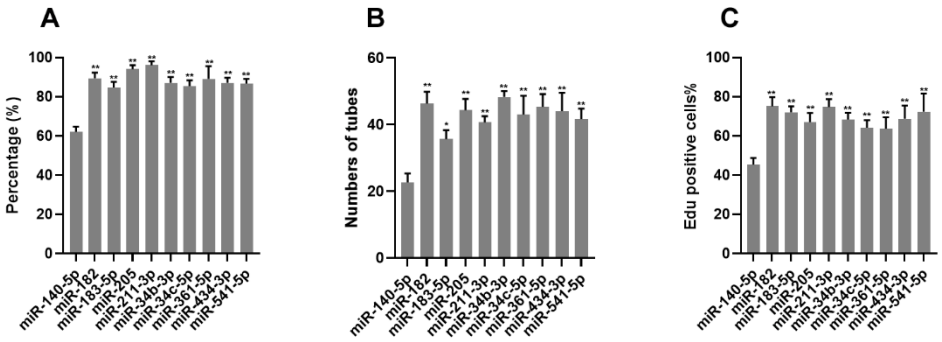

Figure S1. Effect of upregulated miRNAs of 0.5MPa/NCs-exos on angiogenesis. (A) Effect of upregulated miRNAs on migration of HUVECs. Mean±SEM are provided (n=3). *p<0.05, **p <0.01 for comparison with miR-140-5p group. **(B)** Effect of upregulated miRNAs on tube formation ability of HUVECs. Mean±SEM are provided (n=3). *p<0.05, **p<0.01 for comparison with miR-140-5p group. **(C)** Effect of upregulated miRNAs on proliferation of HUVECs. Mean±SEM are provided (n=3). *p<0.05, **p<0.01 for comparison with miR-140-5p group. NCs-exos: notochordal cells-derived exosomes.

Table S1 Primer sequences used in quantitative real-time polymerase chain reaction

Gene symbol	Forward primer	Reverse primer	GenBank ID
brachyury	GAGTGGACCACCTGCTGAGC	GGTGGATGTAGACGCAGCTG	292301
miR-140-5p	GAGTGTCAGTGGTTTTACCCT	GCAGGGTCCGAGGTATTC	406932
miR-U6	GGAACGATACAGAGAAGATTAGC	TGGAACGCTTCACGAATTTGCG	26827

Table 2 Sequences of synthetic miR140-5p mimic/inhibitor

Gene symbol	Sequences (5'-3')
miR-140-5p mimic	CAGUGGUUUUACCCUAUGGUAGACCAUAGGGUAAAACCACUGUU
miR-140-5p inhibitor	AACCCAUGGAAUUCAGUUCUCA